CHEMISTRY
A EUROPEAN JOURNAL

DOI: 10.1002/chem.200700370

Unusual Coexistence of Magnetic and Nonmagnetic Mo_6 Octahedral Clusters in a Chalcohalide Solid Solution: Synthesis, X-ray Diffraction, EPR, and DFT Investigations of $Cs_3Mo_6I^i_6I^i_{2-x}Se^i_xI^a_6$

Kaplan Kirakci,[a] Stéphane Cordier,*[a] Alex Shames,[b] Bruno Fontaine,[a] Olivier Hernandez,[a] Eric Furet,[a] Jean-François Halet,[a] Régis Gautier,[a] and Christiane Perrin[a]

Abstract: The $Cs_3Mo_6I^i_6I^i_{2-x}Se^i_xI^a_6$ series has been obtained by a solid-state route. There is evidence for a solid solution between the compositions $Cs_3Mo_6I^i_6I^i_{0.8}Se^i_{1.2}I^a_6$ and $Cs_3Mo_6I^i_6I^i_{0.4}Se^i_{1.6}I^a_6$ (space group: $R\bar{3}c$, $Z=6$; $a=16.7065(4)$, $c=20.5523(4)$ Å, $V=4967.8(2)$ Å^3 and $a=16.6354(3)$, $c=20.5444(4)$ Å, $V=4923.7(2)$ Å^3, respectively). The structure of this new series is based on magnetic $[Mo_6I^i_6Se^i_2I^a_6]^{3-}$ and diamagnetic $[Mo_6I^i_7Se^iI^a_6]^{3-}$ units with 23 and 24 valence electrons per Mo_6 cluster, respectively. For a particular x, the structure of $Cs_3Mo_6I^i_6I^i_{2-x}Se_xI^a_6$ is based on a mixture of $(x-1)[Mo_6I^i_6Se^i_2I^a_6]^{3-}$ with $(2-x)[Mo_6I^i_7Se^iI^a_6]^{3-}$. This leads to an average $[Mo_6I^i_6I^i_{2-x}Se_xI^a_6]^{3-}$ ionic unit deduced from single-crystal X-ray diffraction investigations. The two inner positions of the average face-capped $[Mo_6I^i_{8-x}Se^i_xI^a_6]^{3-}$ ionic units (located on the threefold axis of the unit) are randomly occupied by iodine and selenium, whereas the other ligand positions are fully occupied by iodine. Low-temperature electron paramagnetic resonance (EPR) studies reveal a signal split into two components with $g_\parallel > g_\perp$. The reciprocal double integration intensity of the EPR signal versus T graph reveals a typical Curie law behavior. A density functional theory (DFT) study indicates that occupation of the inner position on the threefold axis by selenium atoms is preferred energetically among the three possible distributions of selenium atoms. The comparison of experimental and theoretical g values confirms the crystallographic analysis and agrees with the axial elongation of the Mo_6 cluster within the crystal structure.

Keywords: cluster compounds · halides · magnetic properties · molybdenum · solid-state reactions

Introduction

It is known that octahedral molybdenum clusters form $[(Mo_6L^i_8)L^a_6]$ units when they are associated with halogen and/or chalcogen ligands (according to the Schäfer and Schnering notation, superscript i = inner face-capping ligands; superscript a = apical[1–3]). The metal–metal bonding levels of their molecular orbital diagrams are completely filled with 24 metal electrons/cluster (valence electron count (VEC) = 24). The condensation of units through double $L^{a\text{-}i}/L^{i\text{-}a}$ chalcogen bridges (L = S, Se, Te) leads to inorganic solids characterized by disperse band structures owing to their stronger electronic interactions compared with compounds built up from discrete units. Condensed units can have fewer than 24 electrons per Mo_6 cluster; this leads to interesting transport properties (conducting, or even superconducting) as in the $A_xMo_6L_8$ (A = cation; L = S, Se, Te) series, which display a condensation of units through double $L^{i\text{-}a}/L^{a\text{-}i}$ bridges in the three directions of space. The best superconducting behavior is exhibited by $22\,e^-$ per Mo_6 cluster, owing to a high density of states at the Fermi level ($PbMo_6S_8$: VEC = 22 and $T_c = 14$ K).[4]

On the other hand, the magic number rule of 24 electrons per M_6 cluster is the driving force in the formation of discrete M_6L_{14} cluster unit-based compounds. Hitherto, AgW_6Br_{14} with 23 electrons per cluster constitutes the only

[a] K. Kirakci, Dr. S. Cordier, Dr. B. Fontaine, Dr. O. Hernandez, Dr. E. Furet, Dr. J.-F. Halet, Dr. R. Gautier, Dr. C. Perrin
Sciences Chimiques de Rennes
UMR 6226 CNRS-Université de Rennes 1-ENSC Rennes
Avenue du Général Leclerc, F-35042 Rennes Cedex (France)
Fax: (+33) 223-236-799
E-mail: stephane.cordier@univ-rennes1.fr

[b] Dr. A. Shames
Department of Physics, Ben Gurion University of the Negev
P.O.B 653, 84105 Beer Sheva (Israel)

example of an M_6 cluster compound synthesized by solid-state routes that violates this rule.[5]

In this work, we report the solid-state synthesis and the characterization, by powder and single-crystal X-ray diffraction, EPR measurements, and DFT theoretical studies, of $[Mo_6I^i_7Se^iI^a_6]^{3-}$ and $[Mo_6I^i_6Se^i_2I^a_6]^{3-}$ octahedral cluster units that exhibit $24e^-$ and $23e^-$ per Mo_6 unit, respectively. Although $23e^-$ per Mo_6 clusters could be prepared by reaction of liquid bromine with solubilized precursors containing $24e^-$ per Mo_6 cluster,[6] up to now it has never been obtained directly by a solid-state route. $[Mo_6I^i_7Se^iI^a_6]^{3-}$ and $[Mo_6I^i_6Se^i_2I^a_6]^{3-}$ octahedral cluster units make up the basic building blocks of a solid solution with the $Cs_3Mo_6I^i_6I^i_{2-x}Se^i_xI^a_6$ general formula characterized experimentally within the two limit compositions $Cs_3Mo_6I^i_6I^i_{0.8}Se^i_{1.2}I^a_6$ and $Cs_3Mo_6I^i_6I^i_{0.4}Se^i_{1.6}I^a_6$. The structural findings are discussed and compared with those already established for related compounds, namely $Cs_3Mo_6Br^i_7O^iBr^a_6$[7] and $Rb_3Re_6S^i_7Br^iBr^a_6$.[8] Low-temperature EPR studies reveal a signal split into two components with $g_\parallel > g_\perp$. Comparison of experimental and theoretical g values calculated using a relativistic DFT method is in accordance with the structural analysis. Additionally, the DFT study also indicates that among the three possible isomeric distributions of the two selenium atoms on the inner position within the $[Mo_6I^i_6Se^i_2I^a_6]^{3-}$ unit, the occupation of the inner position on the threefold axis is preferred energetically.

Results and Discussion

Structural features: The $Cs_3Mo_6I^i_6I^i_{2-x}Se^i_xI^a_6$ series crystallizes in the trigonal system (space group $R\bar{3}c$) and is related structurally to those of $Cs_3Mo_6Br_{13}O$[7] and $Rb_3Re_6S_7Br_7$.[8] It contains discrete units of average symmetry. Indeed, for a special value of x, the structure is built up from a mixture of $(x-1)[Mo_6I^i_6Se^i_2I^a_6]^{3-}$ and $(2-x)[Mo_6I^i_7Se^iI^a_6]^{3-}$ ionic units with D_{3d} and C_{3v} idealized local symmetry, respectively. This leads to an apparent average $[Mo_6I^i_6I^i_{2-x}Se^i_xI^a_6]^{3-}$ unit (Figure 1) with a local D_{3d} symmetry, deduced from single-crystal X-ray diffraction analysis. The molybdenum cluster is face-capped by eight inner ligands in such a way that two inner ligand positions located on the threefold axis (12*c* Wyckoff position) are randomly occupied by iodine (I1) and selenium (Se1) atoms, whereas the six other inner ligand positions and the six apical ligand positions (36*f* Wyckoff position) are fully occupied by iodine (I3 and I2 atoms, respectively). This results in a molybdenum cluster in which two opposite triangular faces, perpendicular to the ternary axis, are randomly capped by selenium Se1 and iodine I1, whilst the six other triangular faces around the ternary axis are capped by iodine. There is a charge of 3− on both units, so the $[Mo_6I^i_7Se^iI^a_6]^{3-}$ and $[Mo_6I^i_6Se^i_2I^a_6]^{3-}$ units possess $24e^-$ and $23e^-$ per Mo_6, respectively, with one unpaired electron in the metal–metal bonding states in the latter. As developed below, the presence of an Mo_6 cluster with $23e^-$ per Mo_6 unit is supported by EPR evidence. In the mixture of

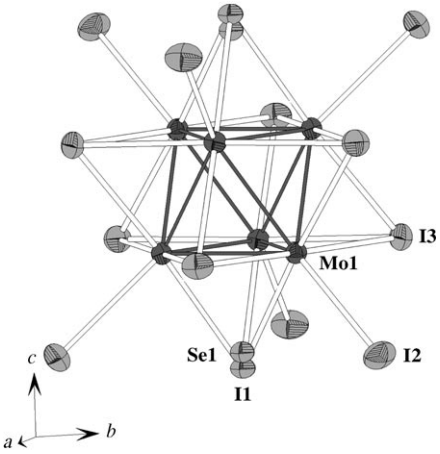

Figure 1. The $[Mo_6I^i_6I^i_{2-x}Se^i_xI^a_6]^{3-}$ unit. Displacement ellipsoids are shown at the 50% probability level. Locally, only one of the two positions Se1 or I1 is occupied.

$23e^-$ and $24e^-$ Mo_6 clusters, one could expect Mo to be in a static random distribution. This assumption is invalidated by the fact that the displacement parameters of molybdenum atoms, refined anisotropically, exhibit a shape very close to an isotropic one. Moreover, no significant residues in the Fourier difference maps are found around the Mo atoms. Similar features have been already observed in Nb_6 fluorobromides and fluoroiodides for which a random distribution of Nb_6 cluster units with different F/Br or F/I ratios lead to an average position of Nb atoms.[9] The $[Mo_6I^i_7Se^iI^a_6]^{3-}$ and $[Mo_6I^i_6Se^i_2I^a_6]^{3-}$ units are arranged in an ABCA′B′C′ close-packed stacking (Figure 2). The layers are strongly compressed along the *c* axis, resulting in short distances between the L1 (I1, Se1) inner ligands (located on the ternary axis) belonging to two adjacent units from layers A and A′.

The refined x values for the three single crystals of general formula $Cs_3Mo_6I^i_6I^i_{2-x}Se^i_xI^a_6$ are 1.22(1), 1.47(2), and 1.65(1); they will be labeled **1**, **2** and **3**, respectively. For **3**, the Se1–Se1 and Se1–I1 distances are 4.024(4) and 3.714(11) Å, respectively. They agree with a simultaneous occupation of two adjacent 12*c* equivalent positions by selenium atoms or with an alternating distribution of iodine and selenium atoms along the threefold axis of the crystal structure. In contrast, the short I1–I1 distance of 3.405(15) Å (less than the sum of the ionic radii of two I^-) forbids the simultaneous occupation of two adjacent 12*c* equivalent positions by two iodine atoms. The Cs1 cation randomly occupies the 18*e* Wyckoff position and the Cs2 cation position is split into the randomly occupied 36*f* Wyckoff position. The refined occupancies are 0.35(5) and 0.32(2) for Cs1 and Cs2, respectively. Cs1 is separated from Cs2 by 0.27(3) Å and Cs2 atoms are separated from each other by 0.28(3) Å. These short distances do not enable the simultaneous occupation of two adjacent sites by cesium atoms, in good agreement with their observed refined occupancies. Each cesium atom is surrounded by four cluster units (Figure 3), belong-

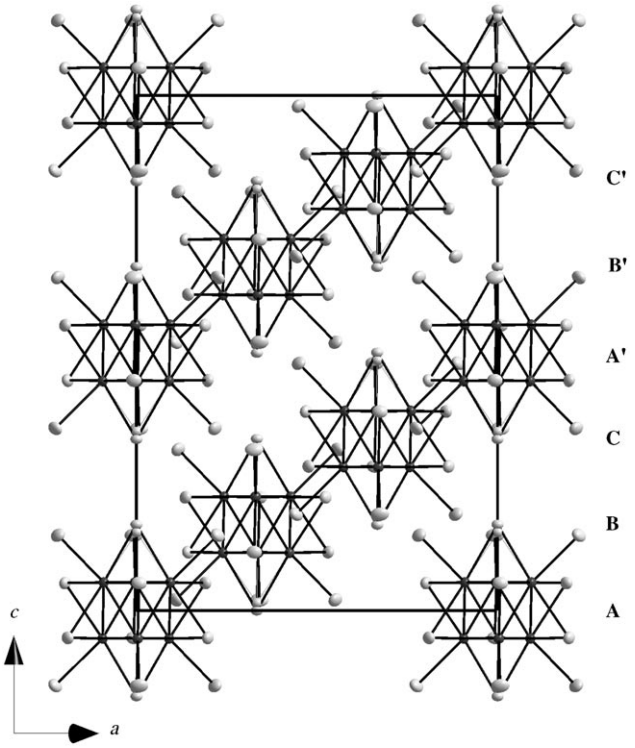

Figure 2. Projection of the $Cs_3Mo_6I^i_6I^i_{2-x}Se^i_xI^a_6$ structure along the [010] direction.

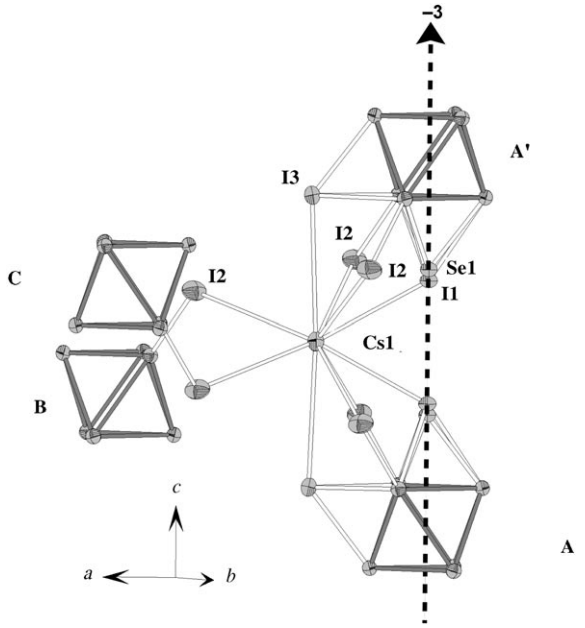

Figure 3. Cs1 environment in $Cs_3Mo_6I^i_6I^i_{2-x}Se^i_xI^a_6$. Displacement ellipsoids are shown at the 50% probability level. Locally, only one of the two positions Se1 or I1 is occupied.

ing to four different layers of the stacking (A, B, C, A′), which build a deformed tetrahedron. The ten-coordinate Cs2 site is built from four apical ligands and four inner ligands belonging to two cluster units from layers A and A′ and from two additional apical ligands belonging to two cluster units from layers B and C. It results in twelve Cs2–I^a interatomic distances (six for each split Cs2 atom) that vary within the range 3.69(2)–4.30(2) Å, four Cs2–I^i interatomic distances (two for each split Cs2 atom) of 4.01(3) and 4.08(3) Å and four Cs2–I^i/Se^i interatomic distances (two for each split Cs2 atom) of 3.71(2) and 3.86(2) Å, respectively, and 3.74(2) and 3.89(2) Å, respectively. The coordination sites of Cs1 and Cs2, being surrounded by the same four cluster units, are almost the same, but with different interatomic distances. Moreover, the short Cs1–I1 interatomic distance of 3.52(1) Å (less than the sum of the ionic radii of Cs^+ and I^-) clearly indicates a correlation between the occupancy of Cs1 and those of Se1 and I1; that is, the occupation of the Cs1 site implies an empty I1 site and an occupied Se1 site (Figure 3). This results in six Cs1–I^a interatomic distances that vary within the range 3.92(1)–4.102(5) Å, two Cs1–I^i interatomic distances of 4.0448(6) Å and two Cs1–Se^i interatomic distances of 3.68(1) Å.

A slight elongation of the unit cell parameters occurs when the structures of **1** and **2** are solved for lower Se contents. This evolution must be attributed to longer Cs–(I, Se) interatomic distances as well as longer L1–L1 interunit contacts rather than to the evolution of the bond lengths within the unit. Indeed, owing to the increase in the number of $[Mo_6I^i_6Se^i_2I^a_6]^{3-}$ units with $23e^-$ per Mo_6 cluster, the average Mo–Mo bond length tends to increase slightly from **1** to **3**, whereas the Mo–(I, Se) distances are almost equal.

The crystal structure of $Cs_3Mo_6I^i_6I^i_{2-x}Se^i_xI^a_6$ is based on the same packing of cations and units as those found in $Cs_3Mo_6Br_{13}O$ or in $Rb_3Re_6S_7Br_7$. However, the structure of the Mo_6 oxybromide is built up of only $[Mo_6Br^i_7O^iBr^a_6]^{3-}$ ionic units with $24e^-$ per Mo_6 cluster, in contrast to $Cs_3Mo_6I^i_6I^i_{2-x}Se^i_xI^a_6$, which contains two types of units with VEC values of 24 or $23e^-$ per Mo_6 cluster. This experimental finding suggests that the lower electronegativities of I and Se compared with those of Br and O would be more favorable when observing lower electronic counts. In $Rb_3Re_6(S^i_5Br^i)S^i_2Br^a_6$, six inner ligand positions are randomly occupied by sulfur and bromine, whilst the two inner ligand positions, lying on the ternary axis, are fully occupied by sulfur. This is the opposite of the arrangement of inner ligands in $Cs_3Mo_6I^i_6I^i_{2-x}Se^i_xI^a_6$. Moreover, the rubidium cation occupies its crystallographic positions fully, in contrast to cesium, the crystallographic position of which is occupied randomly in the title series.

Theoretical considerations: For the octahedral metallic $Mo_6I^i_{10}Se_2I^a_6$ architecture, three isomers can be envisioned, depending on the arrangement of the chalcogen atoms in the inner positions. In order to evaluate the relative stability of the isomers of C_{2v} or D_{3d} symmetry (Figure 4), DFT calculations were first carried out on isolated $[Mo_6I^i_6Se^i_2I^a_6]^{3-}$ isomers with $23e^-$ per Mo_6 cluster. Symmetry constraints (see Figure 4) were taken into account for the geometry optimizations. The results are shown in Figure 5.

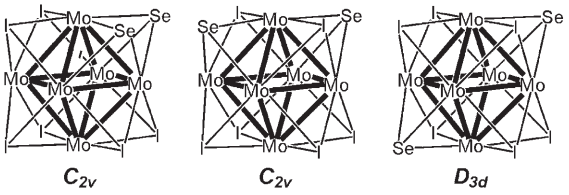

Figure 4. Geometric isomers for a $[Mo_6I^i_6Se^i_2I^a_6]$ cluster core with their point groups. For clarity, apical iodide ligands are not shown.

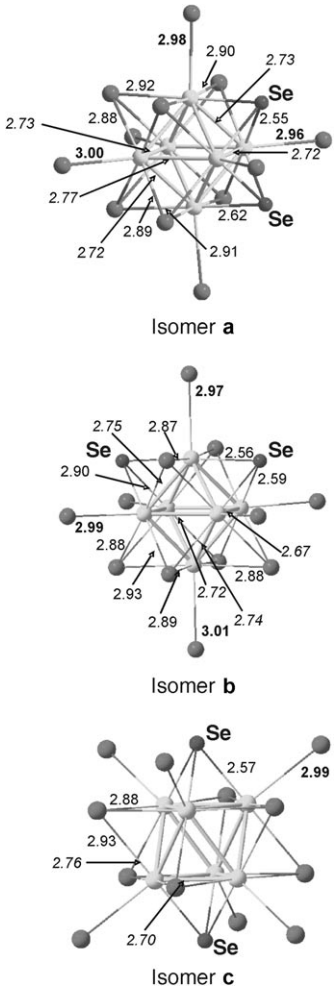

Figure 5. DFT-optimized geometries of $[Mo_6I^i_6Se^i_2I^a_6]^{3-}$ isomers. Mo–Mo (italics), Mo–L^i (standard type), and Mo–L^a (bold) distances are given in Å.

Isomer **c**, in which the two Se atoms are along one threefold axis, is computed to be the most stable. Isomer **a**, in which the two chalcogen atoms lie in a *cis* position with respect to one Mo atom, is slightly less stable (+0.02 eV or 1.8 kJ mol^{-1}), whereas isomer **b**, in which the chalcogen atoms are *trans* with respect to one Mo atom, is 0.13 eV (25 kJ mol^{-1}) higher in energy than isomer **c**. Overall, the Mo–I^a optimized distances are about 0.2 Å greater than the experimental distances. This is explained by the electrostatic interactions caused by the countercations not being included in the calculations. A shortening ($\approx$0.1 Å) is noted for these M–I^a contacts when point charges, used to model the electric field created by the cations around the cluster in the solid, are included in the calculations. Nevertheless, Mo–Mo and Mo–L^i optimized distances compare well with the experimental ones. As shown by Ogliaro et al.[10] for $M_6Cl^i_{12-n}O_nCl^a_6$ octahedral cluster units (M = Nb, Ta; n = 1, 3) in which n chlorine inner atoms are replaced by n oxygen atoms, the presence of two selenium ligands does not change the electronic structure of the octahedral M_6X_{14} halide clusters drastically. Energy diagrams and molecular orbitals (MOs) of these $[Mo_6I^i_6Se^i_2I^a_6]^{3-}$ clusters present the same general features of the electronic structure as M_6L_{14} octahedral clusters: that is, the occurrence of a significant energy gap between the 12 Mo–Mo bonding and nonbonding occupied MOs and the vacant Mo–Mo antibonding MOs for the count of 24 electrons. The highest occupied MOs (HOMOs) of all isomers receive a major contribution from the metal atoms (Figure 6). These HOMOs also contain a significant contribution from the inner selenium atoms (27%, 18% and 25% for **a**, **b** and **c**, respectively), much more than that of iodine inner atoms.

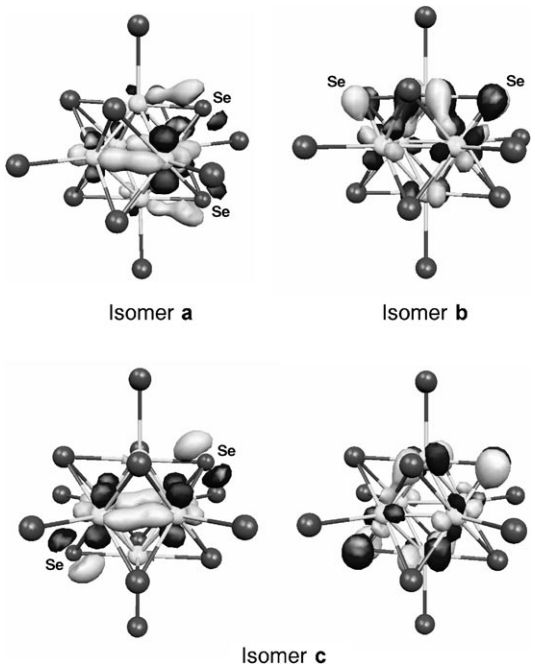

Figure 6. Singly occupied HOMOs of the 23-electron $[Mo_6I^i_6Se^i_2I^a_6]^{3-}$ isomers (the HOMO of isomer **c** is doubly degenerate). Red, purple, and yellow spheres represent Se, I, and Mo atoms, respectively.

The presence of 23-electron $[Mo_6I^i_7Se^iI^a_6]^{2-}$ and 24-electon $[Mo_6I^i_6Se^i_2I^a_6]^{4-}$ clusters was investigated theoretically. Geometry optimizations were carried out on $[Mo_6I^i_6Se^i_2I^a_6]^{4-}$ isomers with 24 electrons. The same energetic trend is observed: that is, **c** is preferred over **a** and **b**. The structural evolution of each optimized isomer is consistent with the

full occupation of the singly occupied HOMOs of the $[Mo_6I^i_6Se^i_2I^a_6]^{3-}$ isomers (Figure 6).

EPR study: Single crystals were selected manually in products from a "$Cs_4Mo_6I_{14.5}Se_{0.5}$"-loaded starting composition and analyzed by the EDXS technique. EPR studies were performed on small nonoriented crystals. At low temperature ($4\,K \le T \le 25\,K$), the spectral pattern is typical of a polycrystalline axially symmetric $S = {}^1/_2$ system with no hyperfine splitting (Figure 7), in agreement with the presence

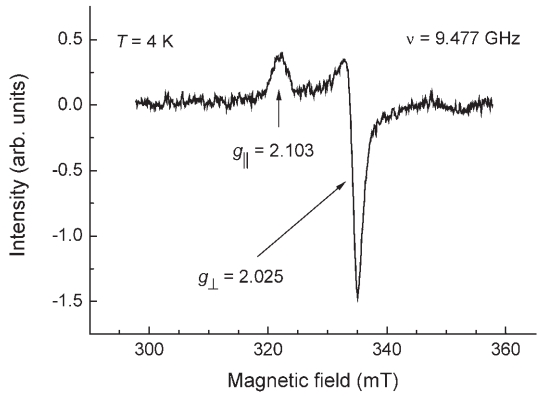

Figure 7. EPR spectrum of $Cs_3Mo_6I^i_6I^i_{2-x}Se^i_xI^a_6$ crystals at $T = 4$ K.

of $[Mo_6I^i_6Se^i_2I^a_6]^{3-}$ units exhibiting one unpaired electron per cluster ($23\,e^-$ per Mo_6). The pattern and, correspondingly, g tensor values are practically unchanged within the temperature range $4\,K \le T \le 25\,K$. The parameter values found ($g_\perp = 2.025 \pm 0.001$, $g_\parallel = 2.103 \pm 0.001$, $g_{av} = 2.05$) are quite close to those found in frozen solutions of $[(Mo_6Cl_7S)Cl_6]^{2-}$ ($23\,e^-$ per Mo_6).[6] However, for the latter compound, the values of the $g_\perp$ and $g_\parallel$ are interchanged. This indicates a difference in the sign of the spin–orbital interaction parameter, which could be caused by another type of axial distortion. In $[(Mo_6Cl_7S)Cl_6]^{2-}$ there is only one S atom per unit, whilst in $Cs_3Mo_6I_6Se^i_xI^a_6$ there are two Se atoms per unit located on the ternary axis of the unit, leading to a unit symmetrically distorted along the threefold axis. Consequently, the g values for these complexes should be such that $g_\parallel > g_\perp$, as is found in most of the axially distorted Cu^{2+} complexes.[11] This corresponds exactly to what we observe, and is supported by the topology of the singly occupied HOMO computed for the isomer **c**. As shown in Figure 6, this latter shows a strong axial anisotropy. The HOMOs of isomers **a** and **b** do not present such an elongated shape.

The graph of the reciprocal double integrated intensity of the EPR signal versus T in the range $4 \le T \le 25$ K exhibited a typical Curie law behavior (Figure 8), implying that the system is magnetically completely dissolved and that there are no (or very weak) intercluster magnetic interactions. This result is in agreement with the stoichiometry and structural data reported here for the title compound.

To compare experimental results obtained from EPR measurements, the g tensor was computed for the three different isomers. Relativistic DFT calculations led to averaged g values of 2.180, 2.193, and 2.088 for isomers **a**, **b**, and **c**, respectively. The best agreement between theory and experiment is obtained for **c**. The slight difference between g_{av} (2.05) measured by EPR experiments and g_{av} calculated for isomer **c** (2.09) is not very significant, considering the level of theory of the computations. On the other hand, the anisotropic g values calculated for isomer **c** (g_{11}, g_{22}, g_{33}: 2.701, 1.873, 1.689, respectively) differ from the g values measured by EPR ($g_\parallel = 2.103$ and $g_\perp = 2.025$). At least two explanations can be given for the origin of these differences. First, g tensor calculation depends strongly on the molecular geometry. Since a precise experimental crystallographic structure of the $[Mo_6I_{12}Se_2]^{3-}$ cluster is not available, calculations of the g tensor for optimized geometry could give rise to deviations. That could also be explained by the fact that the theoretical calculations are performed for a static case, while the EPR experiments could give evidence for some dynamic effect leading to a motional averaging of g values. Consequently, $g_\parallel$ will be smaller than g_{11}, and $g_\perp$ will be greater than g_{22} and g_{33}. This is what we effectively see from EPR measurements. The presence of such a dynamic effect is confirmed by a weak temperature dependence of the g factors: at 24 K $g_\parallel$ reduces slightly to 2.099 and $g_\perp$ increases to 2.027. The origin of this dynamic motion has been unclear up to now.

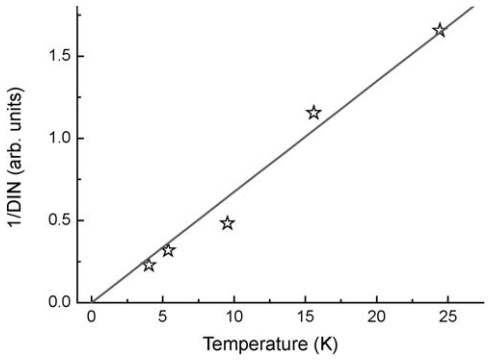

Figure 8. Reciprocal double integration intensity of the EPR signal versus T.

Conclusion

The synthesis and characterization of the $Cs_3Mo_6I^i_6I^i_{2-x}Se^i_xI^a_6$ restricted solid solution between the two compositions $Cs_3Mo_6I^i_6I^i_{0.8}Se^i_{1.2}I^a_6$ and $Cs_3Mo_6I^i_6I^i_{0.4}Se^i_{1.6}I^a_6$ within the range $1.2 \le x \le 1.6$ are reported. For a particular x value, the structure of $Cs_3Mo_6I^i_6I^i_{2-x}Se^i_xI^a_6$ is based on a mixture of $(x-1)[Mo_6I^i_6Se^i_2I^a_6]^{3-}$ and $(2-x)[Mo_6I^i_7Se^iI^a_6]^{3-}$. The $[Mo_6I^i_6Se^i_2I^a_6]^{3-}$ unit contains $23\,e^-$ per Mo_6 cluster and is magnetic, whereas the $[Mo_6I^i_7Se^iI^a_6]^{3-}$ unit contains $24\,e^-$ per Mo_6 cluster and is diamagnetic. Within the structure, the Se atoms are located on the threefold axis of the clusters. The EPR studies exhibited a typical Curie law behavior and a

signal that is typical of axially symmetric $S=1/2$ systems with no hyperfine splitting, in agreement with the presence of $[Mo_6I^i_6Se^i_2I^a_6]^{3-}$ units having one unpaired electron per cluster ($23\,e^-$ per Mo_6). The theoretical analysis revealed that among the possible isomers with the $[Mo_6I^i_6Se^i_2I^a_6]^{3-}$ formula, the isomer with the D_{3d} symmetry is the most stable. This is supported by the calculation of the g tensor using a relativistic DFT method.

Experimental Section

Synthesis of $Cs_3Mo_6I^i_6I^i_{2-x}Se^i_xI^a_6$ and chemical analyses: Powder mixtures (0.5 g) of CsI (Alfa Aesar, 99.9%), Se (Alfa Aesar, 99.99%), Mo (Plansee, 99.95%) and Mo_6I_{12}, prepared according to the procedure described in reference [12a] were ground, compacted and placed in a silica tube. The tube was sealed under vacuum, heated at 950°C, and air-cooled to room temperature. Single crystals of $Cs_3Mo_6I^i_6I^i_{0.5}Se^i_{1.5}I^a_6$ were obtained initially from reactions designed to synthesize the stoichiometric "$Cs_4Mo_6I_{12}Se_2$" chalcoiodide, which is potentially isostructural with $Cs_4Mo_6Br_{12}Se_2$.[12b] After preliminary structural determinations by single-crystal X-ray diffraction, several syntheses were performed with various "$Cs_wMo_6I^i_{8-y}Se^i_yI^a_6$" loaded compositions in order to determine whether the $Cs_3Mo_6I^i_6I^i_{0.5}Se^i_{1.5}I^a_6$ stoichiometry found in these preliminary studies would correspond to a defined composition, or to a particular composition within a phase breadth. After several syntheses as well as combined energy dispersive spectrometry (EDS) and X-ray diffraction analyses of the resulting products, it was found that the Cs/Mo ratio of $Cs_3Mo_6I^i_6I^i_{0.5}Se^i_{1.5}I^a_6$ crystals was constant and equal to 0.5 within the standard uncertainties (s.u's). One could expect that the upper and lower limits for the $Cs_3Mo_6I^i_6I^i_{2-x}Se^i_xI^a_6$ series, corresponding to compounds either based only on $[Mo_6I^i_6Se^i_2I^a_6]^{3-}$ bisubstituted or on $[Mo_6I^i_7Se^iI^a_6]^{3-}$ monosubstituted units, are "$Cs_3Mo_6I_{12}Se_2$" and "$Cs_3Mo_6I_{13}Se$". Then the corresponding stoichiometric equations reaction should be Equations (1) and (2).

$$3\,CsI + {}^{9}/_{12}Mo_6I_{12} + {}^{18}/_{12}Mo + 2Se \rightarrow Cs_3Mo_6I^i_6Se^i_2I^a_6 \quad x=2;\ 23e^-\ \text{per}\ Mo_6 \tag{1}$$

$$3\,CsI + {}^{10}/_{12}Mo_6I_{12} + {}^{12}/_{12}Mo + 1Se \rightarrow Cs_3Mo_6I^i_7Se^iI^a_6 \quad x=1;\ 24\,e^-\ \text{per}\ Mo_6 \tag{2}$$

However, although theoretically achievable, there was no evidence for a continuous solution between these two limit formulas, but only a restricted one between the two compositions $Cs_3Mo_6I^i_6I^i_{0.8}Se^i_{1.2}I^a_6$ and $Cs_3Mo_6I^i_6I^i_{0.4}Se^i_{1.6}I^a_6$ ($x=1.2$ and $x=1.6$). Moreover, pure compounds between the two latter compositions have never been obtained. These findings are explained by the coformation of other stable compounds. First, the excision reaction between 2CsI and Mo_6I_{12} (developed formula $Mo_6I^i_8I^{a-a}_{4/2}I^a_2$) leads easily to the formation of $Cs_2Mo_6I^i_8I^a_6$ containing discrete $[Mo_6I^i_8I^a_6]^{2-}$ units.[12a] Second, an excess of CsI leads to the disproportionation of Mo_6I_{12} leading to Mo and to $Cs_3Mo_2I_9$[13] built from $(Mo_2I_9)^{3-}$ complexes. In addition, Se can react with Mo to give $MoSe_2$. When Se is incorporated in the CsI/Mo_6I_{12} starting mixture, substitution of inner iodine by chalcogen occurs together with excision. These reactions for the lower and upper limits can be written as Equations (3) and (4).

$$3\,CsI + Mo_6I_{12} + Se \rightarrow Cs_3Mo_6I_{13}Se + {}^{1}/_{2}I_2 \quad x=1;\ 24e^-\ \text{per}\ Mo_6 \tag{3}$$

$$3\,CsI + Mo_6I_{12} + 2\,Se \rightarrow Cs_3Mo_6I_{13}Se_2 + I_2 \quad x=2;\ 23e^-\ \text{per}\ Mo_6 \tag{4}$$

From Equations (3) and (4), it can be assumed that excess of I_2 favors the formation of species with higher Mo oxidation states than in Mo_6 clusters ($Cs_3Mo_2I_9$). Therefore, several loaded compositions were prepared and subsequently heated at different temperatures and for various reaction times, with intermediate regrindings and re-annealings, to optimize the experimental procedure. The powder X-ray diffraction analysis showed the reaction to be complete after three days, but longer reaction times (up to seven days) were necessary to obtain single crystals. It was found that an excess of one CsI per Mo_6 in the loaded "$Cs_3Mo_6I_{14-x}Se_x$" composition gives the highest yields of reaction. Too large an excess of CsI favors the formation of $Cs_3Mo_2I_9$ while a deficit favors the formation of $Mo_6I_{10}Se$.[14] A study by powder X-ray diffractometry on samples obtained from several "$Cs_4Mo_6I_{15-y}Se_y$" (CsI + $Cs_3Mo_6I_{14-y}Se_y$) loaded compositions was performed to determine precisely the limits of the homogeneity range of the $Cs_3Mo_6I^i_6I^i_{2-x}Se^i_xI^a_6$ solid solution. The highest reaction yield, determined by Rietveld refinements, was obtained for $y=0.5$.

EDS analysis of single crystals from different preparations with a JEOL JSM 6400 scanning electron microscope equipped with an Oxford Link ISIS EDS microprobe indicated that the crystals contained the expected elements with fluctuations of the Se/I ratio and a constant Cs/Mo ratio of 0.5.

Single-crystal X-ray diffraction studies: Single crystals of $Cs_3Mo_6I^i_6I^i_{2-x}Se^i_xI^a_6$ used for the structural determinations were selected in the syntheses described above. We found the following refined upper and lower limits and intermediate values for x for the three single crystals of **1**, **2**, and **3**: 1.22(1), 1.47(2), and 1.65(1), respectively. The X-ray diffraction data of the single crystals **1**, **2**, and **3** were collected at room temperature on a Nonius KappaCCD area detector X-ray diffractometer with $Mo_{K\alpha}$ radiation ($\lambda=0.71073$ Å; Centre de Diffractométrie de l'Université de Rennes 1, France). For data collection and structure refinement details, see Table 1. The data processing was performed by the KappaCCD analysis software[15] and a semi-empirical absorption correction was applied.[15] The calculation of E statistics[17] performed on the data suggested a centrosymmetric space group. The refinement procedure has allowed retention of the $R\bar{3}c$ centrosymmetric space group among the possible ones deduced from the observed systematic extinctions. Direct methods (program SIR97[18]) yielded a first partial structural solution, including the molybdenum cluster, inner ligands, and cesium cations. Several cycles of refinements (SHELXL-97 program[19]) showed that the iodine inner ligand (I1) located on the 12c Wyckoff position did not fully occupy its position, in contrast to the two other iodine atoms located on two 36f positions. Furthermore, an electronic peak remained close to I1 at a distance from molybdenum corresponding to an Mo–Se bond length.[12b,20] Selenium Se1 was then introduced on this residue with the same atomic displacement parameters as I1. The sum of the occupancies of I1 and Se1 was restricted to the value corresponding to a fully occupied 12c position. Afterward, the first two restraints were relaxed progressively during the convergence, leading to final positions in agreement with reliable Mo–(I, Se) interatomic distances. At this stage, however, Cs1 exhibited unrealistically anisotropic atomic displacement parameters and a residual electronic density peak remained close to this position. Cs2 was then positioned on this peak, corresponding to a 36f Wyckoff position, with the same isotropic atomic displacement parameter as Cs1, and the sum of the occupancies of Cs1 and Cs2 were restricted to the value corresponding to a full 18e Wyckoff position. Subsequently these restraints were relaxed progressively during the convergence, leading to final reliable anisotropic displacement parameters for Cs1 and Cs2. The refined compositions of the three crystals are: $Cs_{3.0(1)}Mo_6I_{12.78(1)}Se_{1.22(1)}$ (**1**), $Cs_{3.0(1)}Mo_6I_{12.53(2)}Se_{1.47(2)}$ (**2**), and $Cs_{3.0(1)}Mo_6I_{12.35(1)}Se_{1.65(1)}$ (**3**), which round to $Cs_3Mo_6I_{12.8}Se_{1.2}$, $Cs_3Mo_6I_{12.5}Se_{1.5}$, and $Cs_3Mo_6I_{12.4}Se_{1.6}$, respectively.

The atomic position parameters and the isotropic equivalent atomic displacement parameters for **1**, **2**, and **3** are reported in Table 2, and relevant interatomic distances are in Table 3 for purposes of discussion.

Further details of the crystal structure investigation can be obtained from the Fachinformationszentrum Karlsruhe, 76344 Eggenstein-Leopoldshafen, Germany (fax: (+49) 7247-808-666; e-mail: crysdata@fiz.karlsruhe.

Table 1. Crystallographic data for $Cs_3Mo_6I_{12.8}Se_{1.2}$ (**1**), $Cs_3Mo_6I_{12.5}Se_{1.5}$ (**2**), and $Cs_3Mo_6I_{12.4}Se_{1.6}$ (**3**); space group $R\bar{3}c$, no.167; $Z=6$; $\lambda=0.71073$ Å).

	1	**2**	**3**
refined formula	$Cs_{3.0(1)}Mo_6I_{12.78(1)}Se_{1.22(1)}$	$Cs_{3.0(1)}Mo_6I_{12.53(2)}Se_{1.47(2)}$	$Cs_{3.0(1)}Mo_6I_{12.35(1)}Se_{1.65(1)}$
formula weight	2692.48	2680.50	2671.86
a (Å)	16.7065(4)	16.6686(3)	16.6354(3)
c [Å]	20.5523(4)	20.5508(4)	20.5444(4)
V [Å^3]	4967.8(2)	4944.9(2)	4923.7(2)
ρ_{calc} [g cm^{-3}]	5.40	5.40	5.41
crystal size [mm^3]	$0.083\times0.084\times0.110$	$0.050\times0.058\times0.073$	$0.091\times0.099\times0.177$
total reflns collected	30679	26443	29080
unique reflns	3013	2805	2894
R_{int} (all reflns)	0.056	0.075	0.055
μ [mm^{-1}]	18.7	18.8	18.9
T [°C]	20	20	20
observed reflns [$I>2\sigma(I)$]	1975	1644	1979
refined parameters	52	52	52
R_1[a] [$I>2\sigma(I)$]	0.033	0.044	0.033
wR_2[a] all data	0.065	0.064	0.073
$\Delta\rho_{min}/\Delta\rho_{max}$ [e Å^{-3}]	−1.55/2.16	−1.40/1.82	−1.73/2.91

[a] $R_1=\Sigma_{hkl}|F_o-F_c|/\Sigma_{hkl}|F_o|$. $wR_2=[\Sigma_{hkl}[w(F_o^2-F_c^2)^2]/\Sigma_{hkl}[w(F_o^2)^2]]^{1/2}$.

de) on quoting the depository numbers CSD-417840 for **1**, CSD-417839 for **2**, and CSD-417838 for **3**.

Powder X-ray diffraction studies: The powder X-ray diffraction patterns of the resulting products from various "$Cs_4Mo_6I_{15-x}Se_x$" (or CsI + $Cs_3Mo_6I_{14-x}Se_x$) loaded compositions were recorded on a Bruker AXS D8 Advance diffractometer (θ–θ Bragg–Brentano geometry) using monochromatic $Cu_{K\alpha_1}$ radiation and a linear position-sensitive detector (Braun L-PSD). A whole-powder-pattern profile fitting procedure without structural constraints (Le Bail refinement, Thompson–Cox–Hastings profile function[21]) was used through FullProf/WinPLOTR[22,23] to refine the unit cell and the profile parameters. Only the powder X-ray diffraction patterns of products obtained with low selenium content in the starting loaded composition could be indexed fully. For "$Cs_4Mo_6I_{14.5}Se_{0.5}$" loaded composition, the coexisting phases (CsI, $Cs_2Mo_6I_{14}$, $Mo_6I_{10}Se$, $Cs_3Mo_2I_9$, and $Cs_3Mo_6I^i_{8-x}Se^i_xI^a_6$) were identified and introduced in the refinement, leading to satisfactory agreement factors. Subsequently, a Rietveld refinement was carried out in order to evaluate the yield of the reaction leading to $Cs_3Mo_6I^i_{8-x}Se_xI^a_6$. Owing to the complexity of the powder X-ray diffraction patterns due to the number of coexisting phases and the induced high degree of accidental overlapping of diffraction lines, combined with the medium instrumental angular resolution, no attempt was made to refine the atomic parameters through this rough analysis, the profile parameters being set to the previously obtained Le Bail refinement values. The refined unit-cell parameters obtained by powder X-ray diffraction for $Cs_3Mo_6I^i_{8-x}Se^i_xI^a_6$ in the mixture obtained with the loaded "$Cs_4Mo_6I_{14.5}Se_{0.5}$" (CsI + $Cs_3Mo_6I_{13.5}Se_{0.5}$) composition ($a=16.692(1)$ Å, $c=20.550(1)$ Å) are very close within the s.u's to the values obtained by single-crystal X-ray diffraction for $Cs_3Mo_6I^i_{6.8}Se^i_{1.2}I^a_6$ ($a=16.7065(4)$, $c=20.5523(4)$ Å). This feature clearly indicates that for the "$Cs^4Mo_6I_{14.5}Se_{0.5}$" loaded composition, the lower limit of the solid-state solution is obtained ($x=1.2$). The rough quantitative phase analysis showed the presence of the following phases and ratios: CsI, 23.7(2)%; $Cs_2Mo_6I_{14}$, 46.3(4)%; $Cs_3Mo_6I^i_{6.8}Se^i_{1.2}I^a_6$, 19.9(2)%; $Mo_6I_{10}Se$, 8.4(3)%; $Cs_3Mo_2I_9$, 1.7(1)%. Owing to the complexity of the powder X-ray diffraction patterns of loaded compositions with higher Se contents, the upper

Table 2. Positional and displacement parameters [Å^2] for **1**, **2**, and **3**.

Atom	Position	x	y	z	Occupancy	U_{eq}
$Cs_3Mo_6I_{12.8}Se_{1.2}$ (**1**)						
Mo1	36*f*	0.66992(2)	0.24321(2)	0.279200(15)	1	0.01971(7)
Se1	12*c*	2/3	1/3	0.1810(3)	0.611(7)	0.0217(7)
I1	12*c*	2/3	1/3	0.1675(3)	0.389(7)	0.0250(9)
I3	36*f*	0.67391(2)	0.143726(19)	0.386645(14)	1	0.03005(7)
I2	36*f*	0.67397(2)	0.11618(2)	0.187962(15)	1	0.03940(9)
Cs1	18*e*	0.8512(15)	1/3	1/12	0.17(4)	0.035(3)
Cs2	36*f*	0.8622(7)	0.3255(13)	0.0802(11)	0.42(2)	0.0559(18)
$Cs_3Mo_6I_{12.5}Se_{1.5}$ (**2**)						
Mo1	36*f*	0.66998(3)	0.24296(3)	0.278883(19)	1	0.01690(9)
Se1	12*c*	2/3	1/3	0.18146(19)	0.735(9)	0.0187(6)
I1	12*c*	2/3	1/3	0.1663(4)	0.265(9)	0.0211(14)
I3	36*f*	0.67403(3)	0.14332(2)	0.386646(16)	1	0.02756(10)
I2	36*f*	0.67397(3)	0.11598(3)	0.187469(18)	1	0.03617(11)
Cs1	18*e*	0.8525(12)	1/3	1/12	0.30(5)	0.033(2)
Cs2	36*f*	0.8605(11)	0.3225(16)	0.0815(16)	0.35(3)	0.049(2)
$Cs_3Mo_6I_{12.4}Se_{1.6}$ (**3**)						
Mo1	36*f*	0.67001(2)	0.24280(2)	0.278677(16)	1	0.01816(7)
Se1	12*c*	2/3	1/3	0.18126(14)	0.823(8)	0.0209(4)
I1	12*c*	2/3	1/3	0.1662(5)	0.177(8)	0.0217(14)
I3	36*f*	0.67410(2)	0.14306(2)	0.386647(14)	1	0.02885(8)
I2	36*f*	0.67402(3)	0.11580(2)	0.187141(15)	1	0.03702(10)
Cs1	18*e*	0.8520(8)	1/3	1/12	0.35(5)	0.0362(13)
Cs2	36*f*	0.8609(8)	0.3240(13)	0.0816(14)	0.32(2)	0.048(2)

Table 3. Selected interatomic distances [Å] in $Cs_3Mo_6I_{12.8}Se_{1.2}$ (**1**), $Cs_3Mo_6I_{12.5}Se_{1.5}$ (**2**) and $Cs_3Mo_6I_{12.4}Se_{1.6}$ (**3**).

	1	2	3	
Mo_6 cluster				
Mo1–Mo1	2.6560(5)	2.6582(7)	2.6582(6)	(×6)
	2.7023(5)	2.7136(7)	2.7200(6)	(×6)
$Mo_6I_{14-x}Se_x$ unit				
Mo1–Se1	2.535(4)	2.523(3)	2.522(2)	(×6)
Mo1–I1	2.761(6)	2.776(7)	2.774(8)	(×6)
Mo1–I3	2.7847(4)	2.7893(5)	2.7912(4)	(×6)
	2.7956(4)	2.7962(5)	2.7948(5)	(×6)
	2.8013(4)	2.8017(6)	2.8003(5)	(×6)
Mo1–I2	2.8581(4)	2.8557(5)	2.8539(5)	(×6)
cesium environment				
Cs1–Se1	3.68(2)	3.696(17)	3.681(12)	(×2)
Cs1–I1	3.53(2)	3.535(19)	3.521(13)	(×2)
Cs1–I3	4.0464(9)	4.0456(8)	4.0448(6)	(×2)
Cs1–I2	3.95(2)	3.921(17)	3.920(12)	(×2)
	3.976(7)	3.972(6)	3.962(4)	(×2)
	4.115(8)	4.112(7)	4.102(5)	(×2)
Cs2–Se1	3.858(13)	3.87(2)	3.856(18)	(×2)
	3.925(15)	3.91(2)	3.892(19)	(×2)
Cs2–I1	3.727(12)	3.72(2)	3.707(18)	(×2)
	3.786(15)	3.75(2)	3.739(18)	(×2)
Cs2–I3	3.98(2)	4.00(3)	4.01(3)	(×2)
	4.11(2)	4.09(3)	4.08(3)	(×2)
Cs2–I2	3.711(14)	3.680(19)	3.686(17)	(×2)
	3.769(13)	3.793(17)	3.782(14)	(×2)
	4.00(2)	3.95(2)	3.95(2)	(×2)
	4.083(18)	4.05(3)	4.06(2)	(×2)
	4.11(2)	4.15(2)	4.12(2)	(×2)
	4.32(2)	4.332(2)	4.30(2)	(×2)
interunit contacts				
Se1–Se1	4.015(9)	4.033(6)	4.024(4)	(×2)
Se1–I1	3.737(9)	3.722(9)	3.714(11)	(×4)
I1–I1	3.460(9)	3.410(12)	3.405(15)	(×2)

limit of the solid solution has not been determined from powder X-ray diffractometry.

Computational details: DFT calculations were carried out using the Amsterdam density functional (ADF) program[24] developed by Baerends and co-workers.[25] Becke exchange[26] and Perdew correlation[27] nonlocal gradient corrections were included in the local density approximation.[28] Geometry optimizations were carried out by the method developed by Versluis and Ziegler.[29] A triple-ζ Slater-type orbital basis set was used for Mo, I, and Se atoms. A single-ζ 5p polarization functions was used for Mo as well as a single a single-ζ 4d polarization function for Se. A frozen-core approximation[26a] was used to treat the core electrons of Mo (1s–4p), I (1s–4p), Se (1s–3d). Spin–orbit relativistic calculations using the zero-order regular approximation (ZORA)[30,31] were performed to determine the calculation of g tensors. The latter were obtained from a nonpolarized-spin wavefunction because spin–polarization effects in spin–orbit coupled equations are difficult to calculate.[32] Since relativistic effects did not show any significant influence on the cluster geometry optimizations, g tensor calculations were carried out on optimized geometries resulting from nonrelativistic calculations. Symmetry was not taken into account in these calculations.

EPR measurements: EPR spectra of several small nonoriented microcrystals were obtained in the 4–25 K range, using a Bruker EMX 8/2.7 spectrometer (X-band, $\nu = 9.5$ GHz) equipped with an Oxford Instruments ESR900 cryogenic unit using liquid helium. EPR spectra were processed and simulated by using Bruker's WIN-EPR and SimFonia software.

Acknowledgements

Dr. T. Roisnel from the Centre de Diffractométrie de l'Université de Rennes 1 is acknowledged for data collection and discussions, as well as Dr. J. Le Lannic and S. Casale from the Centre de Microscopie Electronique à Balayage de l'Université de Rennes 1 for EDS analyses. We are indebted to the French Research Ministry (PECO-NEI (RFR) contract no. 370 and a PhD grant for K.K.) and to the Fondation Langlois for financial support.

[1] H. Schäfer, H.-G. von Schnering, *Angew. Chem.* **1964**, *76,* 833.
[2] C. Perrin, *J. Alloys Compd.* **1997**, *262–263*, 10.
[3] T. G. Gray, *Coord. Chem. Rev.* **2003**, *243*, 213.
[4] R. Chevrel, M. Sergent, *Top. Curr. Phys.* **1982**, vol 32 (Eds.: O. Fischer and M. P. Maple) Springer, p25.
[5] Y. Q. Zheng, H. Borrmann, Y. Grin, K. Peters, H. G. von Schnering, *Z. Anorg. Allg. Chem.* **1999**, *625*, 2115.
[6] M. Ebihara, K. Isobe, Y. Sasaki, K. Saito, *Inorg. Chem.* **1992**, *31*, 1644.
[7] K. Kirakci, S. Cordier, C. Perrin, *C.R. Chim.* **2005**, *8*, 1712.
[8] A. Slougui, A. Perrin, M. Sergent, *J. Solid State Chem.* **1999**, *147*, 358.
[9] a) S. Cordier, O. Hernandez, C. Perrin, *J. Solid State Chem.* **2002**, *163*, 319; b) S. Cordier, C. Perrin, *J. Solid State Chem.* **2004**, *177*, 1017.
[10] F. Ogliaro, S. Cordier, J.-F. Halet, C. Perrin, J.-Y. Saillard, M. Sergent, *Inorg. Chem.* **1998**, *37*, 6199.
[11] J. R. Pilbrow, in *Transition Ion Electron Paramagnetic Resonance*, Clarendon, Oxford, **1990**.
[12] a) K. Kirakci, S. Cordier, C. Perrin, *Z. Anorg. Allg. Chem.* **2005**, *631*, 411; b) S. Cordier, N. Naumov, D. Salloum, F. Paul, C. Perrin, *Inorg. Chem.* **2004**, *43*, 219.
[13] R. Stanger, I. E. Grey, I. C. Madsen, P. W. Smith, *J. Solid State Chem.* **1987**, *69*, 162.
[14] C. Perrin, M. Sergent, F. Le Traon, A. Le Traon, *J. Solid State Chem.* **1978**, *25*, 197.
[15] Nonius COLLECT, DENZO, SCALEPACK, SORTAV: KappaCCD Program Package, Nonius BV, Delft, The Netherlands, **1999**.
[16] G. M. Sheldrick, SADABS version 2.03, Bruker AXS Inc., Madison, WI, USA, **2002**.
[17] R. E. Marsh, *Acta Crystallogr.Sect. B*, **1999**, *51*, 897.
[18] A. Altomare, M. C. Burla, M. Camalli, G. L. Cascarano, C. Giacovazzo, A. Guagliardi, A. G. Moliterni, G. Polidori, R. Spagna, *J. Appl. Crystallogr.* **1999**, *32*, 115.
[19] G. M. Sheldrick, SHELXL-97: Program for the Refinement of Crystal Structure, University of Göttingen, Göttingen, **1997**.
[20] a) R. P. Shannon, *Acta Crystallogr. Sect. A* **1976**, 32, 751; b) K. Kirakci, S. Cordier, C. Perrin, *Chem. Eur. J.* **2006**, *12*, 6419; c) K. Kirakci, S. Cordier, O. Hernandez, T. Roisnel, C. Perrin, *J. Solid State Chem.* **2005**, *178*, 3117.
[21] P. Thomson, D. E. Cox, J. B. Hastings, *J. Appl. Crystallogr.* **1987**, *20*, 79.
[22] J. Rodriguez-Carvajal, FULLPROF: A Program for Rietveld Refinement and Pattern Matching Analysis, *Abstracts of the Satellite Meeting on Powder Diffraction of the XV Congress of the IUCr, Toulouse, France*, **1990**, p127.
[23] T. Roisnel, J. Rodriguez-Carvajal, WinPLOTR: A Windows tool for powder diffraction patterns analysis, in *Proceedings of the Seventh European Powder Diffraction. Conference (EPDIC 7)* (Eds.: R. Delhez, E. J. Mittenmeijer), Materials Science Forum, **2000**, p. 118.
[24] Amsterdam Density Functional (ADF) program, release 2002.03, Vrije Universiteit, Amsterdam (The Netherlands), **2002**.
[25] a) E. J. Baerends, D. E. Ellis, P. Ros, *Chem. Phys.* **1973**, *2*, 41; b) E. J. Baerends, P. Ros, *Int. J. Quantum Chem.* **1978**, *S12*, 169; c) P. M. Boerrigter, G. te Velde, E. J. Baerends, *Int. J. Quantum Chem.* **1988**, *33*, 87; d) G. te Velde, E. J. Baerends, *J. Comput. Phys.* **1992**, *99*, 84.
[26] A. D. Becke, *Phys. Rev. A* **1988**, *38*, 3098.

[27] a) J. P. Perdew, *Phys. Rev. B* **1986**, *33*, 8822; b) J. P. Perdew, *Phys. Rev. B* **1986**, *34*, 7046.
[28] S. H. Vosko, L. Wilk, M. Nusair, *Can. J. Phys.* **1980**, *58*, 1200.
[29] L. Versluis, T. Ziegler, *J. Chem. Phys.* **1988**, *88*, 322.
[30] E. van Lenthe, E. J. Baerends, J. G. Snijders, *J. Chem. Phys.* **1993**, *99*, 4597.
[31] E. van Lenthe, E. J. Baerends, J. G. Snijders, *J. Chem. Phys.* **1994**, *101*, 9783.
[32] E. van Lenthe, E. J. Baerends, J. G. Snijders, *J. Chem. Phys.* **1996**, *105*, 6505.

Received: March 5, 2007
Published online: September 11, 2007

